Effect of Different Nose Profiles on Subsonic Pressure Coefficients

Ryan J. Felkel†
Department of Mechanical and Aerospace Engineering
California State University, Long Beach, Long Beach, CA, 90840

In the past decade, small sounding rockets have become an important educational tool for college aerospace engineering programs. These sounding rockets typically reach high subsonic Mach numbers leading to apogees around 3 to 4 km. It is inevitable that air must speed up to travel around the body which leads to negative forebody pressure coefficients. This paper focuses on the comparison of different nose shapes having cylindrical afterbodies, and selecting the best with the least speed up. Two issues are considered: First, the adverse pressure gradient existing over all cylindrical afterbodies can lead to the separation of a vortex pair at angle of attack that induces rolling moments on the tailfins. Second, if the forebody local Mach number exceeds unity, the flow will decelerate via a shock wave that may also cause a vortex pair to separate at angle of attack. Shock waves are also associated with the onset of wave drag. The key metric used here is the minimum pressure coefficient at the base of the forebody because it drives both the cylinder pressure gradient and the critical Mach number. Three configurations were analyzed: cone-cylinders, ogive-cylinders, and specially shaped forebody-cylinders optimized for minimum pressure coefficient. The optimum forebody shape was found by a cut-and-try approach for a given fineness ratio. Incompressible pressure coefficients were calculated using Munk Airship Theory assuming zero angle of attack. The Karman-Tsien Correction Factor was used with the minimum pressure coefficient to find the critical Mach number. Results are shown as charts of both minimum pressure coefficient and critical Mach number as functions of fineness ratio. These charts reveal that the minimal pressure coefficient increases almost exponentially as fineness ratio increases. The cone-cylinder results show the greatest speed up compared to the other two nose profiles. Ogive-cylinders generate less speeding up and the optimum shape as the least speeding up.

Nomenclature

α	angle of attack
C_p	pressure coefficient
ESRA	Experimental Sounding Rocket Association
γ	specific heat ratio
L/D	fineness ratio
Λ	source strength
M_{cr}	critical Mach
Φ	circumferential angle of cross-section
r	body radius
V_∞	free stream velocity
z	body station

† Undergraduate Student, Experimental Sounding Rockets Association Member, AIAA Member

I. Introduction

Many aerospace projects at a number of universities involve designing, building, and launching experimental sounding rockets, small rockets carrying payloads that perform scientific experiments in a sub-orbital trajectory that reach apogees up to 3 to 4 km. Throughout a trajectory within the atmosphere, it is inevitable that an adverse pressure gradient, that is, pressure increasing with increasing distance from the nose tip, will occur at some point along the forebody of the rocket. Next consider the effect of a small angle of attack that will reduce the pressure on the leeward side of the forebody even more. As the angle of attack is increased, the leeward side adverse pressure gradient becomes more severe eventually inducing boundary layer separation. At the start of leeward side boundary layer separation, a pair of vortices form, one on each side of the body. When the vortex pair moves aft they will induce rolling moments on the tail fins of sounding rockets which can lead to roll lock-in or a catastrophic yaw[3,4]. In roll lock-in the roll rate follows the pitch natural frequency. This prolonged resonance engenders excessive drag and structural loading with extremely adverse consequences to the mission.

There are two causes of an adverse body pressure gradient. First, if local supersonic flow occurs, returning to local subsonic conditions will be done by a normal shock wave. The onset of this phenomenon is when the local surface Mach number reaches unity. The free stream Mach number corresponding to this condition is called the critical Mach number. At higher speeds, the sudden jump to a lower Mach number across a normal shock will be accompanied by a jump in static pressure. Second, since local flow near the body must be faster than free stream, it must continuously return to free stream conditions. This happens at all Mach number. In both cases, the driving consideration is the static pressure at the base of the forebody. The lower this is, the lower the critical Mach number and the greater the negative pressure gradient of the cylindrical afterbody.

The objective of this paper is to show that boundary layer separation can be postponed by the shape of the rocket nose cone. The idea here is to get the incompressible static pressure at the base of the forebody to be as large as possible. This will give the greatest critical Mach number and the least adverse pressure gradient over the cylindrical afterbody. Although vortices cannot be avoided, they can be mitigated by using the best nose cone shape. Shapes that can produce high critical Mach numbers give the greatest Cp with respect to ambient pressure. This is because the closer the Cp local minimum is to 0, the weaker the adverse pressure gradient becomes, which results in a small vortex strength.

This paper's key concept is that while the nose shape does not influence the cross flow pressure distribution[1] at all, that part of the adverse pressure gradient arising from longitudinal flow can be modified by changing the nose shape.

Figure 1 shows the two pressure gradient components. While nothing can be done about the radial adverse pressure gradient (R $\partial p/\partial \Phi$) the longitudinal pressure gradient ($\partial p/\partial z$) can be altered to halt adverse effects as much as one is inclined.

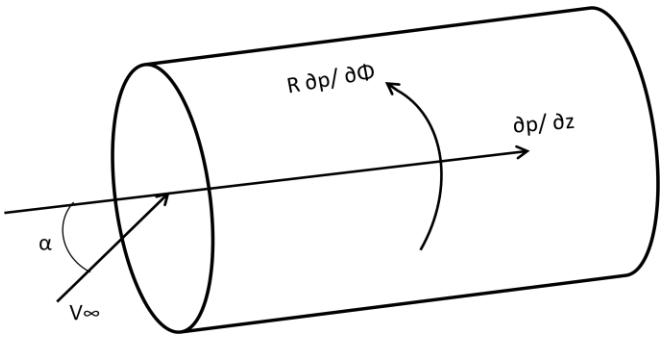

Figure 1 Pressure Gradients

II. Analysis

A system of procedures was used for analysis, as shown in Figure 1, where the dimensions of a nose profile (radius and body station) are inputted and the minimum Cp and critical Mach number are outputted. The nose dimensions are first sent through an incompressible Cp calculation using Munk Airship Theory. From the Munk Airship Theory, a distribution of incompressible pressure coefficients was formed. From this distribution, the minimum pressure coefficient was chosen to run through an incompressible to compressible transformation called the Karman-Tsien Correction, which is valid for subsonic Mach numbers. Then, the isentropic relation between pressure and Mach number was considered, and was integrated into the general equation for the pressure coefficient in order to find where pressure reaches sonic flow, that is, P*. This gives a critical pressure coefficient function in terms of free stream Mach number. This function and the Karman-Tsien Equation are graphed together, and the critical Mach number is where the two curves intersect.

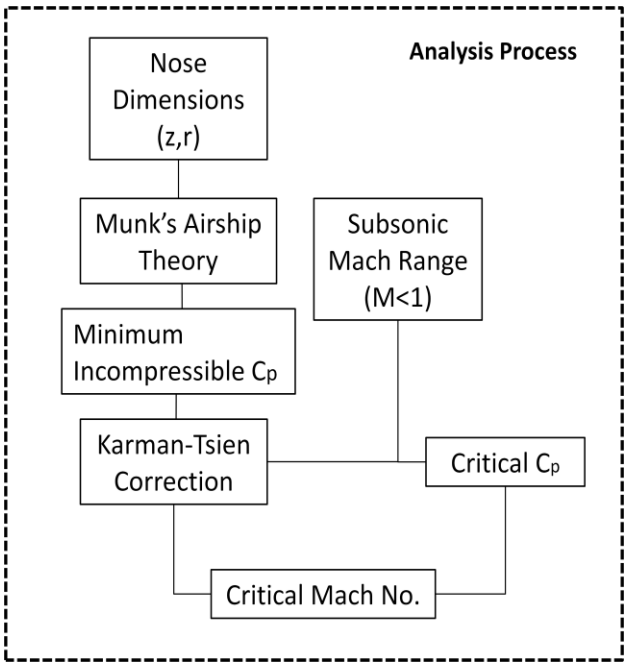

Figure 2 Analysis Process

A. Munk Airship[2] Theory

In order to reveal the effects of pressure along the nose cone, a process called Munk's Airship Theory. Max Munk, the German aerospace engineer who created this theory, used this process to calculate pressure around an elongated airship with a circular cross section. His idea was to consider points along an airship's axis to have source flow, which is depicted in Figure 2.

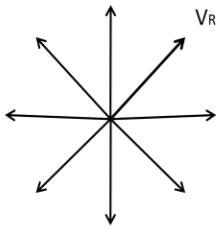

Figure 3 Depiction of Source Flow

The equation for three-dimensional source strength must first be considered, which is given as

$$\Lambda = 4\pi R^2 V_R \quad \text{or} \quad V_R = \frac{\Lambda}{4\pi R^2} \tag{1}$$

Under the assumption that the body is continuous, the mold line is given by r which is in terms of z. The figure shown below shows the R vector and its components. The local source strength is the product of the displacement of the body station (dz_i) and a constant $\sigma(z_i)$.

$$V_R = \frac{\sigma(z_i)dz_i}{4\pi R^2} = \frac{\sigma(z_i)dz_i}{4\pi((z-z_i)^2+r^2)^2} \tag{2}$$

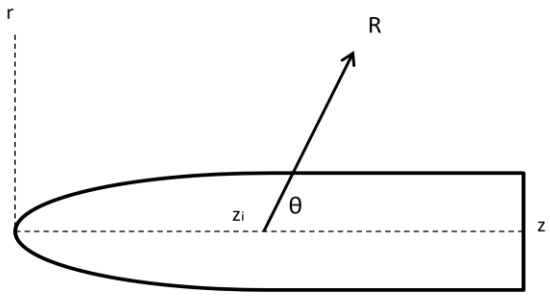

Figure 4 Theoretical Body Mold Line

Under knowledge of the R vector and its components, trigonometry functions can be used to find the equations of radical velocity in terms of r and z.

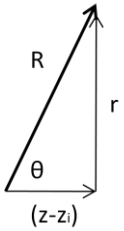

Figure 5 Radial Vector and its Components

$$\sin\theta = \frac{r}{\sqrt{(z-z_i)^2+r^2}} \quad \text{and} \quad \cos\theta = \frac{r}{\sqrt{(z-z_i)^2+r^2}} \tag{3}$$

Now the cylindrical radial and axial velocity components can be evaluated.

$$V_r(z,r) = \frac{1}{4\pi}\int_0^L \frac{r\sigma(z_i)}{((z-z_i)^2+r^2)^{3/2}}\,dz_i \tag{4}$$

$$V_z(z,r) = \frac{1}{4\pi}\int_0^L \frac{(z-z_i)\sigma(z_i)}{((z-z_i)^2+r^2)^{3/2}}\,dz_i \tag{5}$$

If a finite chain of sources are visualized, then it is assumed that radial velocities from different sources will cancel each other out in the z direction, which results in radial flow which can be looked at as discs in finite terms. It is known that the product of the circumferential surface area and its radial velocity is equal to the source strength.

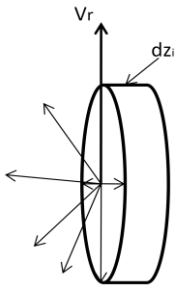

Figure 6 Radial Flow Disc

$$2\pi r dz_i V_r(z,r) = \sigma(z_i)dz_i \quad \text{or} \quad V_r(z,r) = \frac{\sigma(z_i)}{2\pi r} \tag{6}$$

At the point of source analyzed, the free stream velocity and Vr can be juxtaposed to drB/dz since they both have common unit vectors.

$$\frac{V_r(z,r)}{V_\infty} = \frac{dr_B}{dz} \quad \text{or} \quad \sigma(z_i) = 2\pi r \frac{dr_B}{dz} \tag{7}$$

Now consider Bernoulli's incompressible flow equation.

$$P + \frac{1}{2}\rho V^2 = P_\infty + \frac{1}{2}\rho {V_\infty}^2 \tag{8}$$

Using this equation, it can be used to solve for Cp in terms of flow velocity.

$$C_P \equiv \frac{P-P_\infty}{\frac{1}{2}\rho {V_\infty}^2} = 1 - \left(\frac{V}{V_\infty}\right)^2 \tag{9}$$

V is the total magnitude velocity at a given point, which is sum of the radial velocity and the free stream velocity.

$$C_P = 1 - \left(\frac{V}{V_\infty}\right)^2 = 1 - \frac{\left(V_\infty + V_z(z,r)\right)^2 + V_r(z,r)^2}{{V_\infty}^2} = 1 - \frac{{V_\infty}^2 + 2V_z(z,r)V_\infty + V_z(z,r)^2 + V_r(z,r)^2}{{V_\infty}^2} \tag{10}$$

Equation 10 applies as long as the angle of attack vanishes. For a small angle of attack there is an additional term in the Cp equation arising from circumferential cross flow. This additional term acts to depress the leeward side pressure even further, below its zero α value. It follows that the leeward side adverse pressure gradient is the most severe, and that, therefore, boundary layer separation and vortex pair formation starts on the leeward side.

For slender bodies, second order terms would be much smaller than first order terms. Therefore, the second-order terms are neglected. Also,

$$C_P = \frac{-2V_z(z,r)}{V_\infty} \tag{11}$$

The integral equation for Vz and $\sigma(z_1)$ is then substituted,

$$C_P(z,r) = -\int_0^L \frac{(z-z_i)r(z_i)\frac{dr_B}{dz}}{((z-z_i)^2+r^2)^{3/2}} dz_i \tag{12}$$

B. Karman-Tsien Compressibility Correction[1]

A pressure coefficient distribution has now been obtained for an incompressible flow. The next step is to figure out where a critical Mach number would occur. Again, it is important to know if sonic flow occurs because higher speeds would cause a normal shock along the body. Before we can find the critical Mach number, we must consider the body in compressible flow. The Karman-Tsien Compressibility Correction was used to find the compressible Cp. The Cp for incompressible flow, Cp_o, which is found from the output of Munk's Theory, is plugged into Karman-Tsien. The empirically derived formula for Karman-Tsien's equation is:

$$C_P = \frac{C_{P0}}{\sqrt{1-M^2} + \frac{C_{P0}}{2}\left(1-\sqrt{1-M^2}\right)} \tag{13}$$

This correction factor can be used to find the pressure distribution in compressible flow at different free stream Mach numbers. For example, Figure 7 shows the effect of compressibility on the pressure distribution. Note that the minimum Cp occurs at the base of the nose (36"). This is true for all shapes studied.

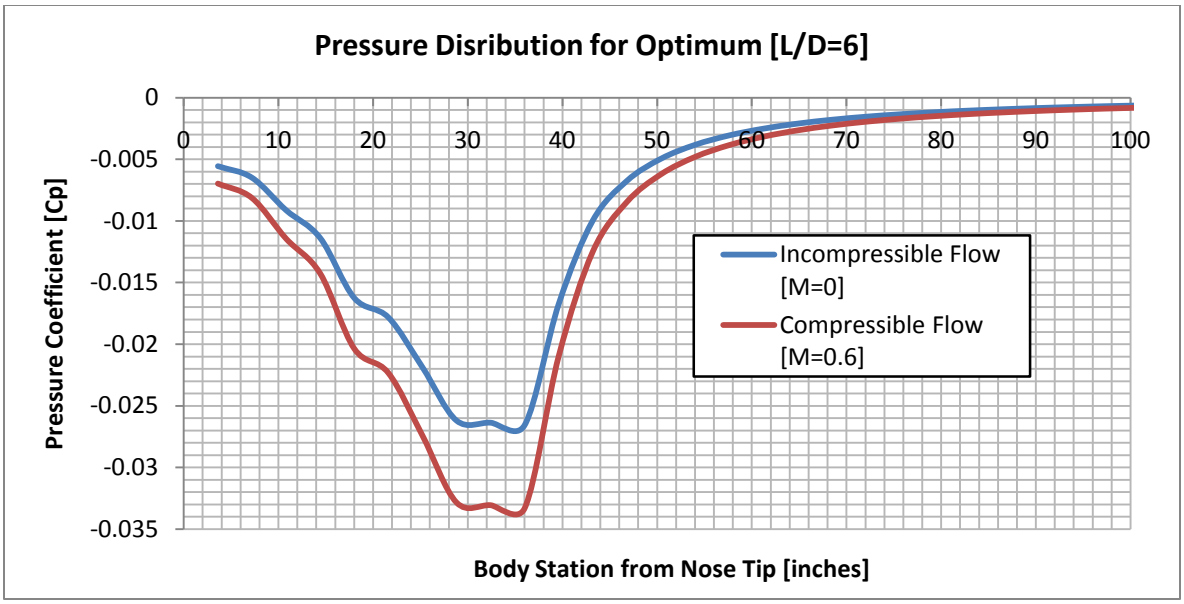

Figure 7 Optimum Pressure Coefficients [L/D=6]

C. Critical Mach Number

The compressible pressure distribution function in terms of Mach number is now known. Now the next step is to find where along this curve the critical Mach number occurs. The equation below shows the general formula for pressure coefficient, which can be rewritten showing a pressure ratio.

$$C_P = \frac{P-P_\infty}{½\gamma P_\infty M_\infty^2} = \frac{2}{\gamma M_\infty^2}\left(\frac{P}{P_\infty} - 1\right) \tag{14}$$

The isentropic relation between pressure and Mach number is known as

$$\frac{P}{P_\infty} = \left[\frac{1+½(\gamma-1)M^2}{1+½(\gamma-1)M_\infty^2}\right]^{\frac{-\gamma}{(\gamma-1)}} \tag{15}$$

Since the interest is to know where the local Mach number reaches unity, a relation between pressure when Mach is 1, and the free steam pressure is utilized. The isentropic relation is then simplified to

$$\frac{P^*}{P_\infty} = \left[\frac{½(\gamma+1)}{1+½(\gamma-1)M_\infty^2}\right]^{\frac{-\gamma}{(\gamma-1)}} \tag{16}$$

The pressure ratio is a function of the free stream Mach number which is plugged into the definition of the pressure coefficient equation. Figure 8 shows what Cp should be at a certain free stream mach number for the critical Mach number to occur.

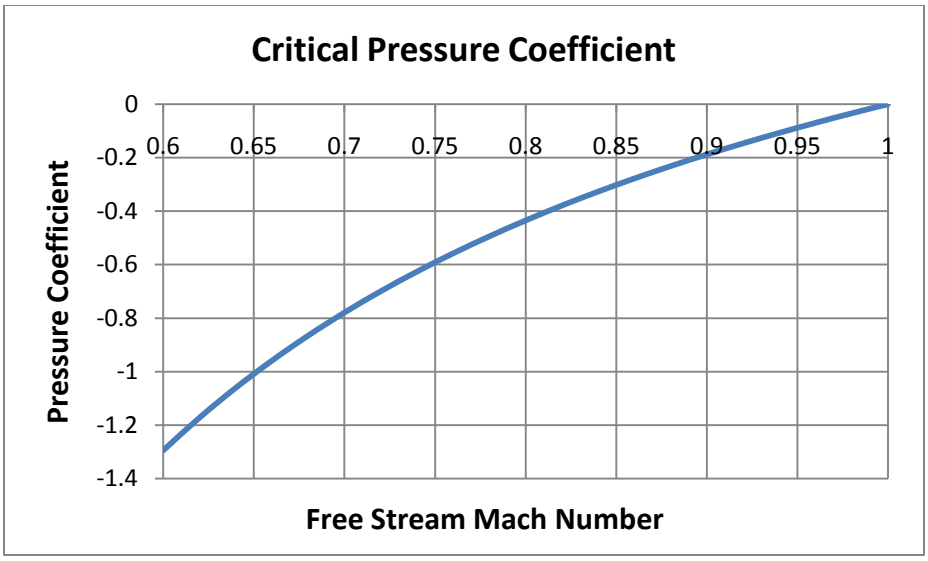

Figure 8 Critical Pressure Coefficient

III. Results

The analysis process was done for three nose shapes with cylindrical afterbodies: a cone, a tangent ogive, and an optimum nose shape developed using cut and try methods. For each shape, different fineness ratios (L/D) shapes were analyzed from 3 to 6, which means for a 36 inch long nose, base radii from 3 in to 6 inches were analyzed. The profiles and Cp distribution along the nose bodies are shown in Fig. 9 and 10 below:

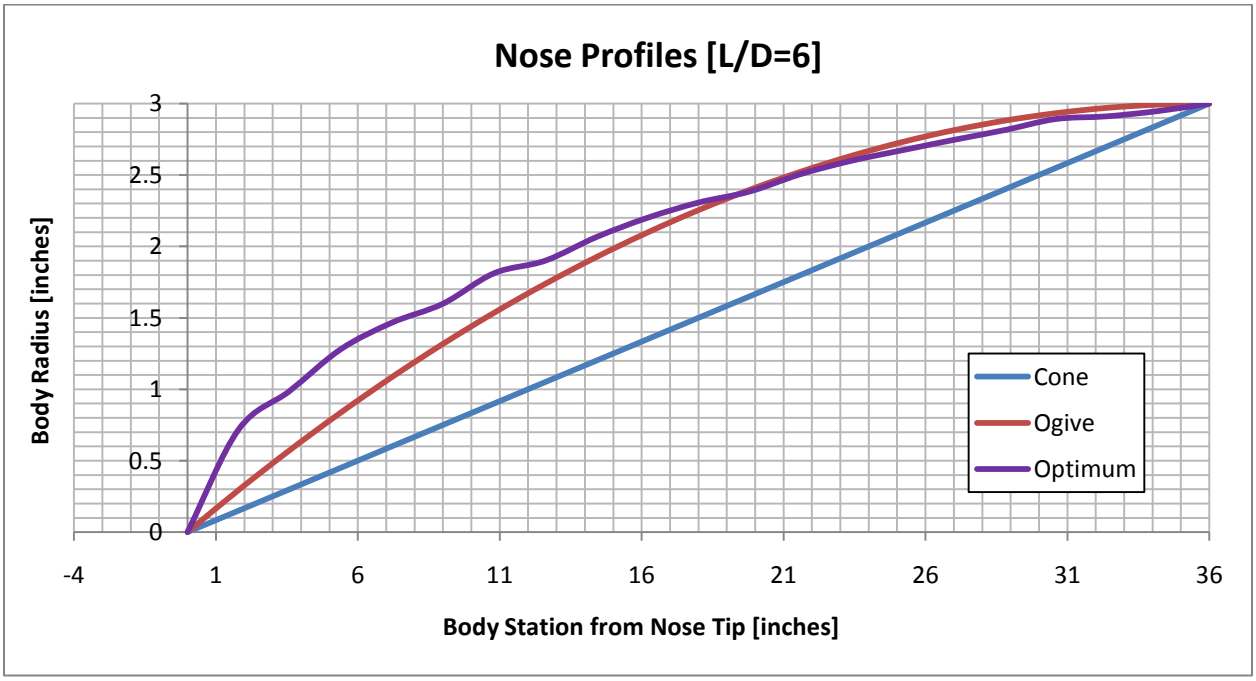

Figure 9 Nose Profiles with a Fineness Ratio of 6

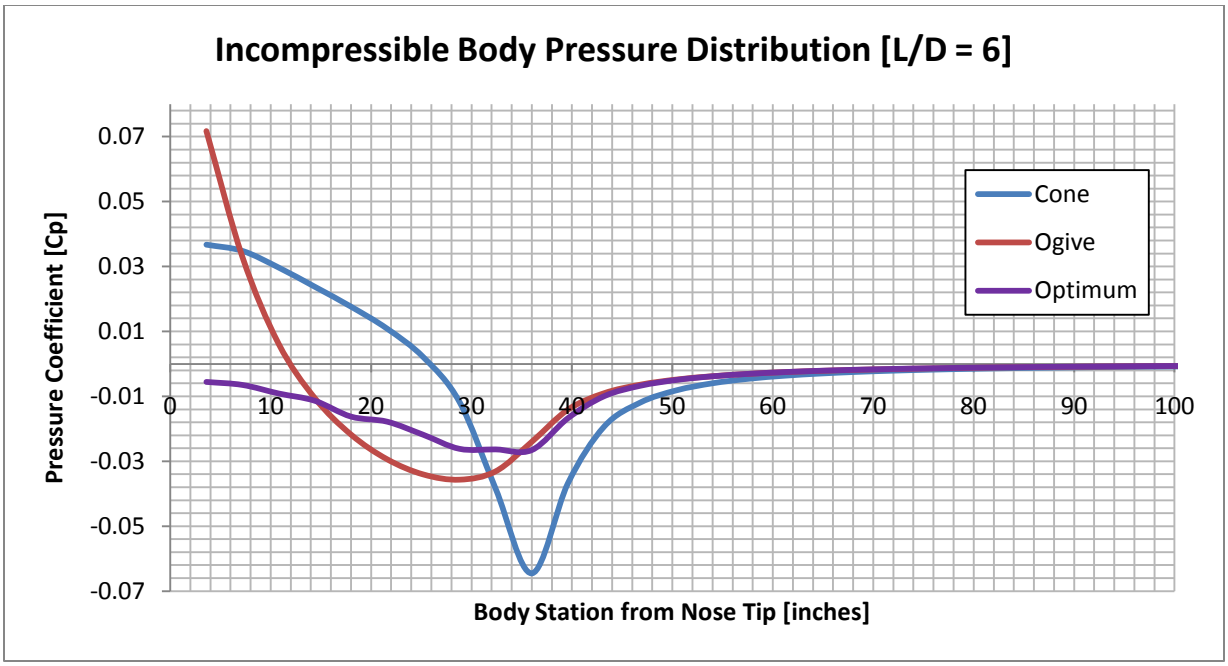

Figure 10 Incompressible Body Pressure Distribution with a Fineness Ratio of 6

The outputs of the analytical process are the minimum pressure coefficient and the critical Mach number, which were plotted in two separate graphs in respect to L/D. The following results are obtained:

Table 1 Analysis Results

R, in	L/D	Mcr Cone-Cylinder	Mcr Ogive	Mcr Optimum	Cp min Cone	Cp min Ogive	Cp min Optimum
6.0	3.00	0.873	0.895	0.915	-0.11706	-0.08616	-0.06278
5.5	3.27	0.878	0.903	0.924	-0.10916	-0.07782	-0.05401
5.0	3.60	0.885	0.910	0.930	-0.10097	-0.06940	-0.04667
4.5	4.00	0.891	0.917	0.937	-0.09246	-0.06092	-0.04061
4.0	4.50	0.897	0.925	0.943	-0.08359	-0.05243	-0.03551
3.5	5.14	0.906	0.934	0.949	-0.07432	-0.04398	-0.02929
3.0	6.00	0.914	0.943	0.953	-0.06454	-0.03566	-0.02656

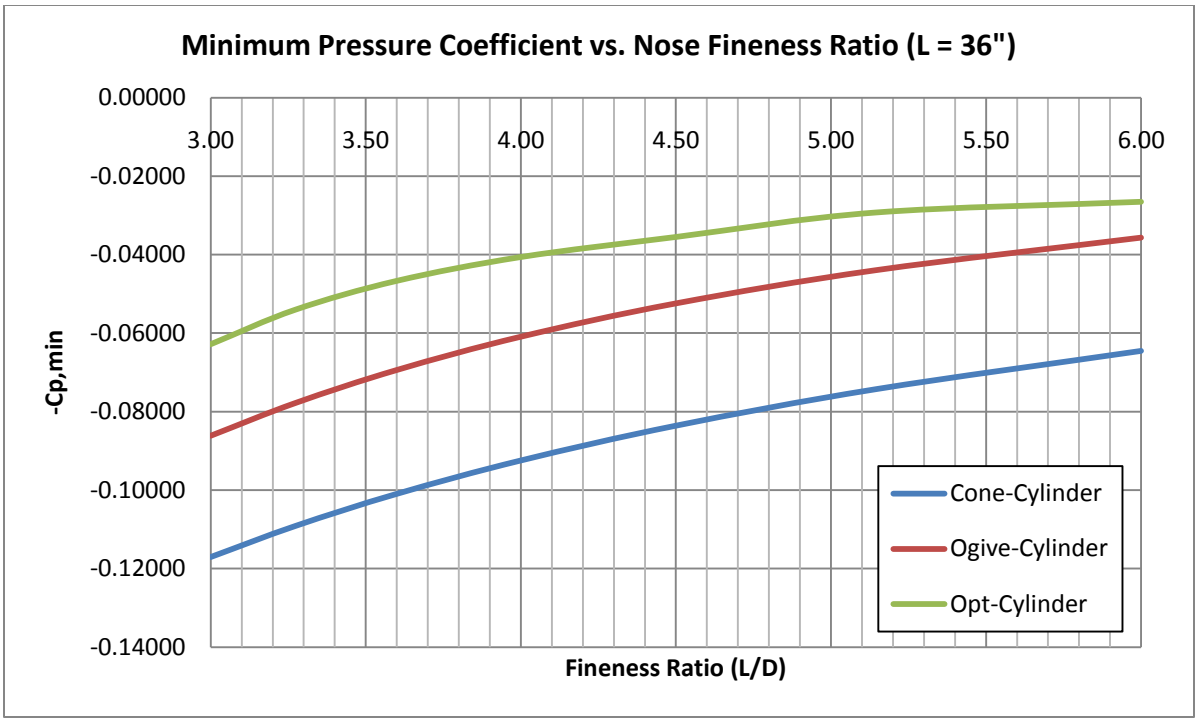

Figure 11 Minimum Pressure Coefficient Versus Nose Fineness Ratio

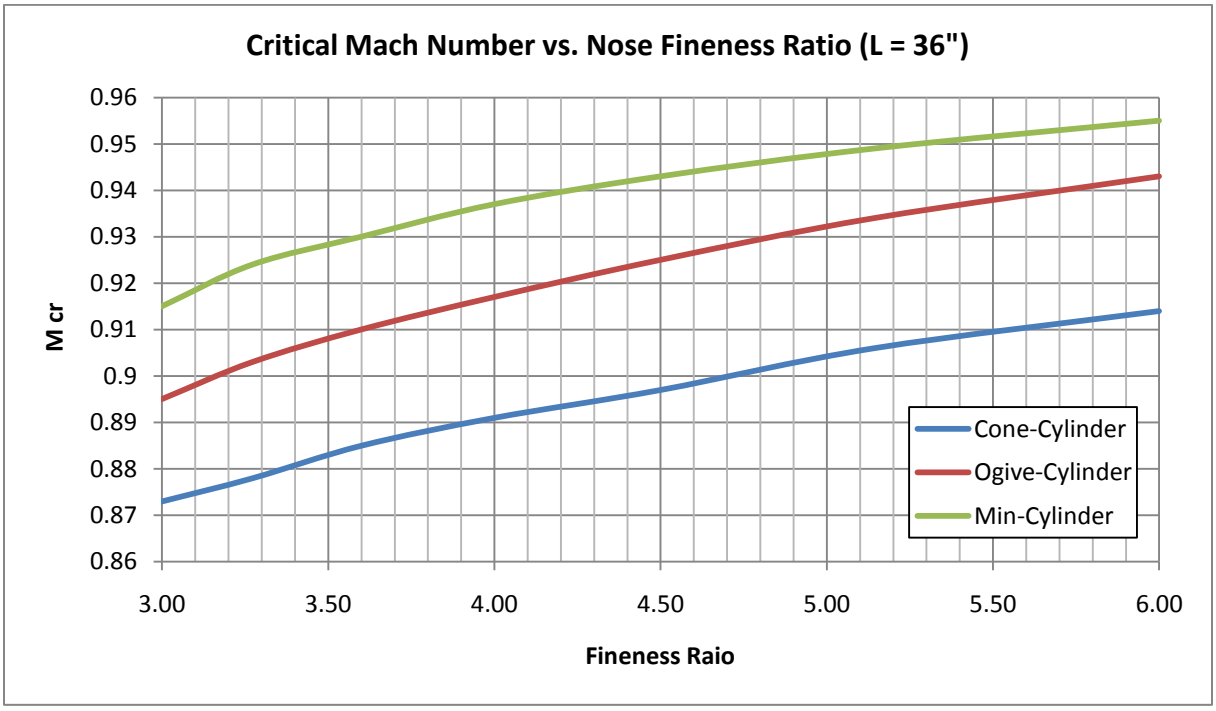

Figure 12 Critical Mach Number Versus Nose Fitness Ratio

IV. Summary

The idea that was set here is to delay boundary layer separation by pushing the critical Mach number as far up as possible. This paper explained the process on how to observe the compressibility effects on a cylindrical nose of a rocket. A body profile was generated and was analyzed using Munk's Airship Theory to get an incompressible pressure distribution profile. The worst case minimum pressure coefficient was chosen and plugged into the Karman-Tsien Correction Factor to find the compressible pressure coefficient that intersects with the critical pressure coefficient function to find the corresponding critical Mach number. This process was one for three different types of noses: a cone-cylinder, ogive-cylinder, and an optimum-shaped-cylinder. Of course, the process of finding the minimum pressure coefficient and critical Mach number is not limited to only these three shapes; this process can apply to any shape of a rocket nose. As long as the shape is continuous, a good estimate of the compressibility effects can be found. The author encourages other rocket teams, and possibly companies in the industry, to use this paper as reference for rocket nose selection.

Acknowledgements

The author would like to give his deepest thanks to Mr. Charles Hoult and Dr. Janet Cameron Hoult for their kindness, patience, and generosity towards the advising of this paper. The author would also like to thank all his peers in the Experimental Sounding Rocket Association (ESRA).

References

[1]: Anderson, J. D., *Fundamentals of Aerodynamics*, 4th ed., Mc Graw-Hill, Boston

[2]: Munk, M. M., *The Aerodynamic Forces on Airship Hulls*, National Advisory Committee for Aeronautics, Report No. 184

[3]: Nicolaides, J. D., *Two Non-Linear Problems in the Flight Dynamics of Modern Ballistic Missiles*, Bureau of Naval Weapons, Washington., D.C., 2004

[4]: Nicolaides, J. D., *On the Free Flight Motion of Missiles Having Slight Configurational Asymmetries*, Army Ballistic Research Laboratories, Aberdeen Proving Ground, MD, 2004